

JLAB-THY-00-16

# LATTICE GAUGE THEORY - QCD FROM QUARKS TO HADRONS<sup>a</sup>

D. G. RICHARDS

*Jefferson Laboratory, MS 12H2, 12000 Jefferson Avenue, Newport News,  
VA 23606, USA*

*Department of Physics, Old Dominion University, Norfolk,  
VA 23529, USA  
E-mail: dgr@jlab.org*

Lattice Gauge Theory enables an *ab initio* study of the low-energy properties of Quantum Chromodynamics, the theory of the strong interaction. I begin these lectures by presenting the lattice formulation of QCD, and then outline the benchmark calculation of lattice QCD, the light-hadron spectrum. I then proceed to explore the predictive power of lattice QCD, in particular as it pertains to hadronic physics. I will discuss the spectrum of glueballs, exotics and excited states, before investigating the study of form factors and structure functions. I will conclude by showing how lattice QCD can be used to study multi-hadron systems, and in particular provide insight into the nucleon-nucleon interaction.

## 1 Lattice QCD: the Basics

### 1.1 Introduction

The fundamental forces of nature can be characterised by the strength of the interaction: gravity, the weak interaction, responsible for  $\beta$ -decay, the electromagnetic interaction, and finally the strong nuclear force. All but the weakest of these, gravity, are incorporated in the Standard Model of particle interactions.

The Standard Model describes interactions through gauge theories, characterised by a local symmetry, or gauge invariance. The simplest is the electromagnetic interaction, with the Abelian symmetry of the gauge group  $U(1)$ . The model of Glashow, Weinberg and Salam unified the electromagnetic and weak interactions through the a broken symmetry group  $SU(2) \otimes U(1)$ . The strong interaction is associated with the unbroken non-Abelian symmetry group  $SU(3)$ , and is accorded the name Quantum Chromodynamics (QCD).

The strength of the electromagnetic interaction is characterised by the dimensionless fine-structure constant  $\alpha_e \simeq 1/137$ . A very powerful calculational technique is to expand as a series in  $\alpha_e$  - perturbation theory. QCD

---

<sup>a</sup>Lectures given at the 14th. Annual Hampton University Graduate Studies at CEBAF, 1st. to 18th. June, 1999

is characterised by a strong coupling constant  $\alpha_s \simeq \mathcal{O}(1)$ . QCD, however, is asymptotically free, with an effective running coupling  $\alpha_s(Q^2)$  decreasing logarithmically with increasing  $Q^2$ . Thus processes with an energy scale large compared with the natural scale of the strong interaction, of the order of the proton mass, are often amenable to the techniques of perturbation theory.

At energy scales of the order of the proton mass, perturbation theory fails. Yet a quantitative understanding of QCD is crucial both for the study of the strong interaction, and for the study of the other forces which are masked by the strong interaction. In this energy regime, we can either employ low-energy effective models of QCD, or seek some way of performing a quantitative calculation directly within QCD. Lattice QCD is the only means we have of performing such an *ab initio* calculation.

Before proceeding to a description of lattice QCD, it is useful to make a comparison between the properties of QCD and of QED:

QED	<i>vs.</i>	QCD
<i>Gauge particle</i>	Photon, $\gamma$	Gluon, $G$
<i>Coupling to</i>	Electric charge, $Q$	Colour charge
<i>Charged particles</i>	$e, \mu, u, d, s\dots$	Quarks, $u, d, s\dots, G$
<i>Photon is neutral</i>		<i>Gluon has colour charge</i>

The gluon self-coupling reflects the non-Abelian, and highly non-linear, nature of QCD. Where are the quarks? They are bound into the colour-singlet hadrons we observe in nature. Lattice gauge theory provides the means to relate the quark degrees of freedom with the observed hadronic degrees of freedom.

## 1.2 Lattice Gauge Theory

Lattice gauge theory was proposed by Ken Wilson in 1974.<sup>1</sup> Because of the gluon self-coupling, we have a sensible pure-gauge theory of interacting gluons, even without quark, or matter, fields. We will consider this theory first.

We begin by formulating QCD in Euclidean space, which we accomplish by a Wick rotation from Minkowski space,

$$t \rightarrow \tau \equiv it. \quad (1)$$

The gauge fields are defined through

$$A_\mu(x) = A_\mu^a(x)T^a, \quad (2)$$

where the  $T^a, a = 1, \dots, 8$  are the generators of  $SU(3)$ , satisfying

$$[T^a, T^b] = if_c^{ab} T^c \quad (3)$$

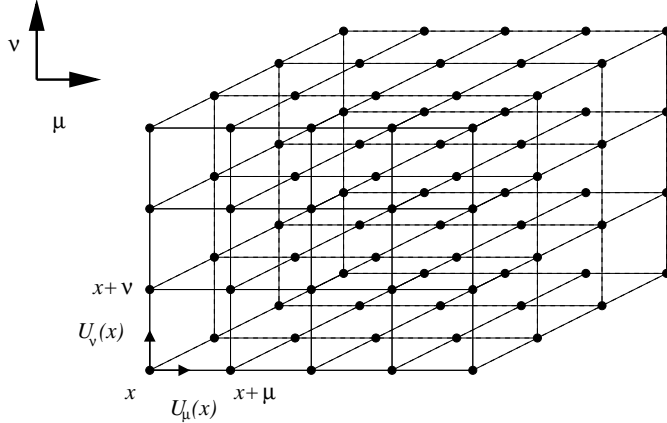


Figure 1: A schematic of a lattice showing the association of the SU(3) matrices  $U_\mu(x)$  with the links of the lattice.

$$\text{Tr } T^a T^b = \frac{1}{2} \delta_{ab}. \quad (4)$$

We now introduce the field-strength tensor

$$F_{\mu\nu}^a \equiv \partial_\mu A_\nu^a - \partial_\nu A_\mu^a + g f^{abc} A_\mu^b A_\nu^c, \quad (5)$$

in terms of which the Euclidean continuum action is

$$S = \frac{1}{4} \int d^4x s F_{\mu\nu}^a F_{\mu\nu}^a. \quad (6)$$

As we will see later, the crucial property of Euclidean space QCD for the formulation of lattice gauge theories is that the action is real. Gauge invariance is manifest through invariance under the transformation

$$A_\mu(x) \rightarrow \Lambda(x) A_\mu(x) \Lambda^{-1}(x) - \frac{1}{ig} (\partial_\mu \Lambda(x)) \Lambda^{-1}(x). \quad (7)$$

We proceed to the lattice formulation of QCD by replacing a finite region of continuum space-time by a discrete four-dimensional lattice, or grid, of points. The gluon degrees of freedom are represented by SU(3) matrices  $U_\mu(x)$  associated with the links connecting the grid points, as shown in Figure 1. We work with the elements of the group, rather than elements of the algebra,

and the SU(3) matrices  $U_\mu(x)$  are related to the usual continuum gauge fields through

$$U_\mu(x) = \exp ig a \int_0^1 dt A_\mu(x + ta\hat{\mu}), \quad (8)$$

where  $g$  is the coupling constant, and  $a$  the lattice spacing. Under a gauge transformation  $\Lambda(x)$ , the link variables transform as

$$U_\mu(x) \rightarrow \Lambda(x)U_\mu(x + \hat{\mu})\Lambda^{-1}(x), \quad (9)$$

in analogy with Eq. 7. Wilson's form of the lattice gauge action is constructed from the elementary plaquettes<sup>1</sup>

$$U_{\square_{\mu\nu}}(x) = U_\mu(x)U_\nu(x + \hat{\mu})U_\mu^\dagger(x + \hat{\nu})U_\nu^\dagger(x). \quad (10)$$

The plaquettes are clearly gauge invariant, and the action is then written

$$S_G = \frac{2N_c}{g^2} \sum_x \sum_{\mu>\nu} \left[ 1 - \frac{1}{N_c} \Re \text{Tr } U_{\square_{\mu\nu}}(x) \right] \equiv -\frac{\beta}{N_c} \sum_x \sum_{\mu>\nu} \Re \text{Tr } U_{\square_{\mu\nu}}, \quad (11)$$

where we have ignored the constant term, and introduced

$$\beta = \frac{2N_c}{g^2}$$

with, for QCD,  $N_c = 3$ . It is straightforward to show that the Wilson lattice gauge action is related to the continuum counterpart, Eq. (6), by

$$S_G = \frac{1}{4} \int d^4x F_{\mu\nu}^a F_{\mu\nu}^a + \mathcal{O}(a^2), \quad (12)$$

so that the lattice gauge action has  $\mathcal{O}(a^2)$  discretisation errors.

### 1.3 Observables and Lattice Gauge Simulations

Within lattice gauge theory, the expectation value of an observable  $O$  is given by the path integral

$$\langle O \rangle = \frac{1}{Z} \int \mathcal{D}U O(U) e^{-S_G(U)} \quad (13)$$

where

$$\mathcal{D}U = \prod_{x,\mu} dU_\mu(x) \quad (14)$$

and  $Z$  is the generating functional

$$Z = \int \mathcal{D}U e^{-S_G(U)}; \mathcal{D}U = \prod_{x,\mu} dU_\mu(x). \quad (15)$$

Before proceeding further, we need to define what we mean by the integration over a group variable  $dU$ . We do this through the Haar measure, which for a compact group is the unique measure having the following properties:

1.

$$\int_G dU f(U) = \int_G dU f(VU) = \int_G dU f(UV) \quad \forall V \in G.$$

2.

$$\int_G dU = 1.$$

This choice of measure respects gauge invariance. Note that, because we are employing the compact variables,  $U_\mu(x)$ , rather than the elements of the algebra, we do not need to fix the gauge, and indeed in most circumstances we do not do so. However, there are cases where working in a fixed gauge is useful, most notably in lattice perturbation theory, where gauge fixing is essential, in the definition of hadronic wave functions, where it is often useful to work in Coulomb gauge, and most directly in the study of the fundamental gluon and quark Green functions of the theory.

On a finite lattice, the calculation of observables is equivalent to the evaluation of a very high, though finite, dimensional integral. In principle, we could estimate this integral by evaluating the integrand at uniformly distributed points. This, however, would be hopelessly inefficient; the exponential behaviour ensures that the integral is dominated by regions where the action is small. Instead we use importance sampling, and generate gauge fields with a probability distribution

$$e^{-S_G(U)}. \quad (16)$$

The interpretation of this exponential in terms of a probability distribution requires that the action be real, and hence the need to work in Euclidean space. The formulation follows that of many systems in statistical physics.

#### 1.4 Statistical and Systematic Uncertainties

##### Statistical Uncertainties

Observables in lattice QCD calculations arise from a Monte Carlo procedure, and thus have statistical uncertainties. Once we have reached thermalisation,

these uncertainties decrease as the square root of the number of configurations, providing successive configurations are sufficiently widely separated to be statistically independent.

### Systematic Uncertainties

Of even greater delicacy than the statistical uncertainties are the systematic uncertainties that enter our computations. These arise from a variety of sources, including:

- *Finite Volume*: Our box must be sufficiently large that finite volume effects are under control. For light hadron spectroscopy, box sizes of at least 2 fm are necessary to ensure that the hadron is not “squeezed”, but for excited states even larger volumes may be required. In addition, the requirement that the spatial extent of the lattice be large compared with the correlation length, set by the pseudoscalar mass, sets a still more stringent constraint at the physical pion mass.
- *Discretisation Effects*: Increasing the inverse coupling  $\beta$  corresponds to progressing to weaker coupling, and hence smaller lattice spacing  $a$ . We must ensure that  $\beta$  is sufficiently large that the scale-breaking discretisation errors are under control, and in practice we perform calculations at several values of  $a$  and extrapolate to the limit  $a = 0$ .

We will encounter several other potential sources of systematic errors when we discuss the inclusion of the quarks.

### 1.5 Including the Quarks

The full generating functional for lattice QCD with a single flavour of quark is

$$Z = \int \mathcal{D}U \mathcal{D}\psi \mathcal{D}\bar{\psi} e^{-S_G(U) + \sum_{x,y} \bar{\psi}(x) M(x,y,U) \psi(y)}, \quad (17)$$

where  $M(x, y, U)$  is the fermion matrix which, in its “naïve” form, is

$$M(x, y, U) = m \delta_{x,y} + \frac{1}{2} \sum_{\mu} \gamma_{\mu} (U_{\mu}(x) \delta_{y,x+\hat{\mu}} - U_{\mu}^{\dagger}(x - \hat{\mu}) \delta_{y,x-\hat{\mu}}) \quad (18)$$

with  $m$  the quark mass. Because the fermion fields are represented by Grassmann variables, we can integrate out the fermion degrees of freedom, to obtain

$$Z = \int \mathcal{D}U \det M(U) e^{-S_G(U)}. \quad (19)$$

The determinant fluctuates rapidly between configurations. Thus it is not sufficient for a Monte-Carlo procedure to generate configurations with probability  $e^{-S_G(U)}$ , and only include the determinant in the calculation of observables;  $\det M(U)$  must be included in the measure. Furthermore, whilst multiplication by the fermion matrix  $M$  involves only nearest neighbour communication, the evaluation of  $\det M(U)$  is essentially a global operation. Thus  $\det M(U)$  must be re-evaluated every time we update even a single value link variable  $U_\mu(x)$ . The most efficient algorithms for the simulation of QCD with dynamical quarks, such as the Hybrid Monte Carlo algorithm,<sup>2</sup> involve a non-local updating procedure. Nevertheless, calculations with dynamical quarks are at least 1000 times as expensive as pure gauge calculations.

The computational overhead of completely including the quark degrees of freedom has encouraged many calculations to be performed in the quenched approximation to QCD, in which we set

$$\det M \equiv 1,$$

in Eq. (19). This corresponds to suppressing the contribution of closed quark loops in the path integral. There are two justifications for this seemly radical approximation. Firstly, the phenomenological observation that the neglect of the quark loops corresponds to the neglect of OZI-suppressed processes. Secondly, the quenched approximation emerges in the large  $N_c$  limit of QCD, where  $N_c$  is the number of colours.

### 1.6 Fermion doubling and chiral symmetry

Unfortunately, the lattice formulation of fermions presents a further challenge. To illustrate how this arises, let us consider the momentum-space fermion propagator

$$M_{xy}^{-1} = \int_0^{\frac{\pi}{a}} \frac{d^4 p}{(2\pi)^4} \frac{e^{ip \cdot (x-y)}}{m + i \sum_\mu \gamma_\mu \sin ap_\mu}. \quad (20)$$

In the massless limit, the propagator has a pole not only at  $p_\mu = 0$ , but also at the edges of the Brillouin zone  $p_\mu = \pi/a$ . Thus in four dimensions, we have a theory with  $2^4$  non-interacting, equal mass fermions. This situation is a consequence of the Dirac equation being first order. Historically, there have been two solutions to this problem.

## Wilson Fermions

Wilson proposed the addition of a second derivative term, or momentum-dependent mass term, to the action:

$$S_F^W = \sum_x \left\{ (m + 4r) \bar{\psi}(x) \psi(x) - \frac{1}{2} \sum_{\mu} [\bar{\psi}(x)(r - \gamma_{\mu}) U_{\mu}(x) \psi(x + \hat{\mu}) + \bar{\psi}(x + \hat{\mu})(r + \gamma_{\mu}) U_{\mu}^{\dagger}(x) \psi(x)] \right\}. \quad (21)$$

In the continuum limit, we find

$$S_F^W = \int d^4x \bar{\psi}(x) (D + m - \frac{arD^2}{2}) \psi(x) + \mathcal{O}(a^2). \quad (22)$$

The addition of the second derivatives lifts the mass of the unwanted doublers, but at a price. We have added  $\mathcal{O}(a)$  discretisation errors to the fermion matrix, and furthermore the additional term explicitly breaks chiral symmetry at any non-zero value of the lattice spacing, though it is important to remember that chiral symmetry is restored in the continuum limit. The breaking of chiral symmetry has the unfortunate consequence that the fermion masses are subject to an additive mass renormalisation. In simulations, it is conventional to reparameterise the fermion matrix as

$$M_{x,y} = (m + 4r) \{ \delta_{x,y} 1 - \kappa \times \text{"hopping term"} \} \quad (23)$$

where the hopping parameter

$$\kappa \equiv \frac{1}{2(4r + m)} \quad (24)$$

is now a tunable parameter, reflecting the additive quark-mass renormalisation. The critical value of the hopping parameter,  $\kappa_{\text{crit}}$ , is that value for which the pion mass vanishes.

## Kogut-Susskind Fermions

The second approach, due to Kogut and Susskind, regards the complete loss of chiral symmetry at finite  $a$  as too great a sacrifice, and therefore aims to preserve a remnant of chiral symmetry whilst reducing the flavour-doubling problem. This formulation leads to four flavours of quark, but the different flavour and spin components are assembled from fields at the sixteen corners of

a  $2^4$  hypercube. While the Kogut-Susskind formulation has been extensively employed in the calculation of quantities where chiral symmetry is crucial, the problematic flavour identification means that I will concentrate on the results using the Wilson formulation in these lectures.

### Chiral Fermions and the Ginsparg-Wilson Relation

Is it possible to construct a formulation that does indeed possess a symmetry analogous to chiral symmetry at a finite lattice spacing, whilst admitting the correct spectrum of quark states? Let us list four properties desired of the free fermion action, which we write in the form

$$S_F = a^4 \sum_x \bar{\psi}(x) D(x, y) \psi(y)$$

1.  $D(x, y)$  is local
2. Far below the cut-off,  $D(p) \simeq i\gamma_\mu p_\mu + \mathcal{O}(p^2)$ .
3.  $D(p)$  is invertible at all non-zero momenta.
4.  $\gamma_5 D + D\gamma_5 = 0$ .

The last two requirements require explanation; 3 demands that the only poles occur at zero momentum, and hence that there be no doublers, whilst 4 is just a statement of chiral symmetry. The famous Nielsen-Ninomiya “no-go” theorem<sup>3</sup> states that it is not possible to find a Dirac operator that allows all four requirements to be satisfied simultaneously, and since the first two requirements were deemed sacrosanct either chiral symmetry had to be broken, or flavour-doubling had to be accepted.

The recent revolution in our understanding of chiral fermions are related to the rediscovery of the Ginsparg-Wilson relation<sup>4</sup>

$$\gamma_5 D + D\gamma_5 = aD\gamma_5 D, \quad (25)$$

as a replacement for requirement 4. At non-zero distances, the Dirac operator does indeed commute with  $\gamma_5$ , and a symmetry, reducing to chiral symmetry in the continuum limit, is preserved even at non-zero values of the lattice spacing. The problem is finding a formulation of the Dirac operator that does indeed satisfy the relation of Eq. 25.

Recently, two formulations satisfying this relation have been discovered. In the case of Domain Wall fermions<sup>5,6</sup> (DWF), an auxiliary fifth dimension,

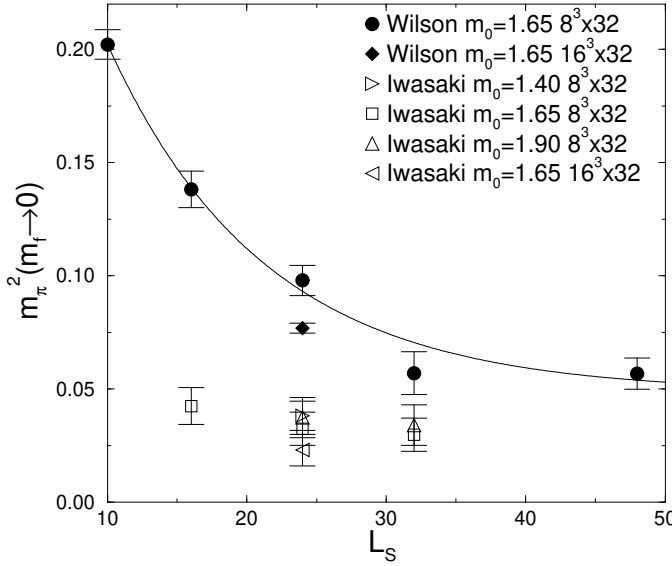


Figure 2: The residual pion mass  $m_\pi^2$  as a function of the extent  $L_s$  of the fifth dimension in the DWF formulation.<sup>7</sup> The calculation is performed in the quenched approximation to QCD, and *Wilson* and *Iwasaki* refer to the standard Wilson gauge action, and an improved gauge action respectively.

with coordinate  $s$  and extent  $N_s$ , is introduced. The action is essentially a five-dimensional Wilson fermion action

$$S_F^{\text{DWF}} = \sum_{x,y,s,s'} \bar{\psi}(x) (D(x,y) \delta_{s,s'} + D^5(s,s') \delta_{x,y}) \psi(y), \quad (26)$$

where  $D(x,y)$  is the usual Wilson-Dirac operator introduced in Eq. 21, but with a *negative* mass term  $M$ . The operator in the fifth dimension,  $D^5(s,s')$ , couples the boundaries through a parameter  $-m$ , which is proportional to the usual four-dimensional quark mass; note that no gauge links are introduced in the fifth dimension. The chiral limit corresponds to  $L_s \rightarrow \infty$ , and then  $m \rightarrow 0$ ; following the former of these limits, the quark mass is only multiplicatively renormalised.

A crucial issue is how small a value of  $L_s$  is sufficient to maintain good chiral properties whilst minimising the computational cost. For the case of hadronic physics, perhaps more important than having good chiral properties

is being able to perform simulations at sufficiently small quark mass for the pion cloud to emerge. Fig. 2 shows the residual pion mass in the chiral limit as a function of function of  $L_s$ .<sup>7</sup>

The second approach is the Overlap formalism, introduced by Narayanan and Neuberger<sup>8,9</sup> Here the overlap-Dirac operator satisfying the property 4 is

$$D^N = \frac{1}{2}(1 + \mu + (1 - \mu)\gamma_5) \frac{H(m)}{\sqrt{H(m)H(m)}} \quad (27)$$

where  $H(m)$  is the Hermitian Wilson-Dirac fermion operator, with negative mass  $m$ , defined by  $H = \gamma_5 D$  where  $D$  is the usual Wilson-Dirac operator. The parameter  $\mu$  is related to the physical quark mass. In this case, the extra computational cost comes not from computing in five dimensions, but rather from evaluating the step function

$$\epsilon(H) = \frac{H}{\sqrt{HH}}. \quad (28)$$

The relative computational overheads of the two implementations is the subject of intense investigation,<sup>10</sup> but in any case the overhead compared to the standard Wilson fermion action is considerable. Whilst this overhead is justified for chiral gauge theories, the situation in the case of hadronic physics is less clear; perhaps there are more efficient ways of approaching physical values of the light-quark masses.

### 1.7 Improvement

The addition of the Wilson term to the fermion action has introduced  $\mathcal{O}(a)$  discretisation errors; in contrast the gauge action has only  $\mathcal{O}(a^2)$  discretisation errors. Thus there has been an emphasis on reducing the errors in the fermion sector through the addition of higher dimensional terms to the action, the improvement programme of Symanzik.<sup>11</sup> In the case of the Wilson fermion action, the leading  $\mathcal{O}(a)$  errors can be removed through the addition of a single dimension-five operator, the magnetic moment, or clover term, proposed by Sheikholeslami and Wohlert<sup>12</sup>

$$S_F = S_F^W - i \frac{c_{SW}\kappa}{2} \sum_{x,\mu,\nu} \bar{\psi}(x) F_{\mu\nu}(x) \sigma_{\mu\nu} \psi(x). \quad (29)$$

The name “clover” is clear from the natural lattice discretisation of  $F_{\mu\nu}$  illustrated in Figure 3.

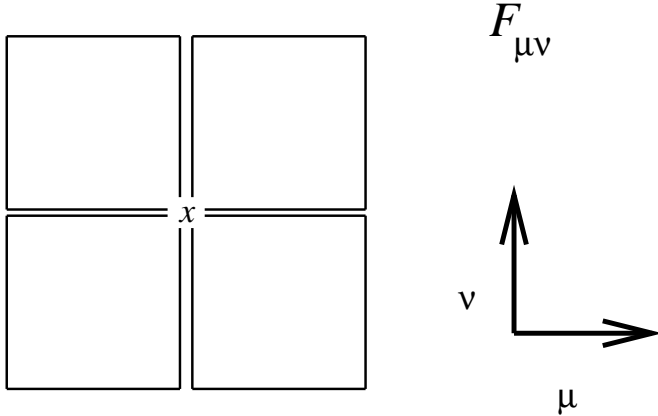


Figure 3: The lattice discretisation of the field-strength  $F_{\mu\nu}(x)$  in terms of the plaquettes with corners at  $x$

Using tree-level perturbation theory, the clover coefficient  $c_{\text{SW}}$  is unity, and the discretisation errors on hadron masses and, with an appropriate discretisation of operators, on-shell matrix elements are formally  $\mathcal{O}(ag^2)$ .<sup>13</sup> UKQCD performed an extensive investigation of the hadron spectrum and hadronic matrix elements using this value of  $c_{\text{SW}}$ , and the discretisation errors, particularly for systems containing heavy quarks, can be substantial.<sup>14</sup>

More recently, two prescriptions for determining  $c_{\text{SW}}$  have been proposed with the aim of reducing discretisation errors still further. In the first, the clover coefficient is constrained to its mean-field-improved, or tadpole, value<sup>15</sup>

$$c_{\text{SW}} = \text{TAD} = \frac{1}{u_0^3} \quad (30)$$

where

$$u_0 = \left\langle \frac{1}{3} \text{Tr} U_{\square} \right\rangle \quad (31)$$

is an estimate of the mean-value of the link variable  $U_{\mu}$ . Though formally the discretisation errors remain  $\mathcal{O}(ag^2)$ , this prescription recognises the poor behaviour of naive lattice perturbation theory arising from the “tadpole” contributions, and attempts to resum the dominant higher-order contributions through the use of a more physical expansion parameter.

The second prescription<sup>16,17</sup> determines  $c_{\text{SW}}$  non-perturbatively in such a way as to remove *all*  $\mathcal{O}(a)$  discretisation errors from hadron masses, and,

with an appropriate choice of operators, from all on-shell matrix elements<sup>18</sup>

$$c_{\text{SW}} = \text{NP} = \frac{1 - 0.656g_0^2 - 0.152g_0^4 - 0.054g_0^6}{1 - 0.922g_0^2}, \quad g_0^2 \leq 1, \quad (32)$$

where  $g_0^2 = 6/\beta$ .

We end this section by remarking that the chiral-fermion formulations are already  $\mathcal{O}(a)$ -improved; the  $\mathcal{O}(a)$  discretisation are introduced through the chiral-symmetry-breaking Wilson term.

## 2 The light-hadron spectrum

The calculation of the spectrum of hadrons containing the light quarks (u,d,s) is the benchmark calculation of lattice QCD; we know many of the results! It also provides a useful theatre for discussion of some of the issues I raised in the introduction. However, let us begin with one of the simplest observations we can make in lattice QCD, that of the linear confining potential.

### 2.1 The Static Quark Potential and Quark Confinement

The simplest observable we can obtain from a lattice simulation is the potential between two (infinitely heavy) static quarks. We construct the Wilson loops

$$W(R, T) = \langle \text{Tr } U(C(R, T)) \rangle \quad (33)$$

where  $U(C(R, T))$  is the product of gauge links around a  $R \times T$  space-time loop. At large times, we can extract the potential  $V(R)$  between two static quarks  $Q$  at separation  $R$ , using

$$W(R, T) \xrightarrow{T \rightarrow \infty} e^{-T V(R)}. \quad (34)$$

An area-law decay of the large Wilson loops is characteristic of a linear, confining potential in QCD, giving rise to a constant force with increasing separations  $r$ . We parameterise this force  $F(r)$  by

$$F(r)r_0^2 = 1.65 + \frac{\pi}{12} \left( \frac{r_0^2}{r^2} - 1 \right) \quad (35)$$

where  $r_0 \simeq 0.5$  fm is a phenomenological parameter<sup>19</sup> which we use to determine the scale. We show this force for the pure-gauge theory, corresponding to the quenched approximation, in Figure 5. At large separations we see the constant force indicative of confinement. But there is a further important observation. The results from all three calculations lie on a single curve, even

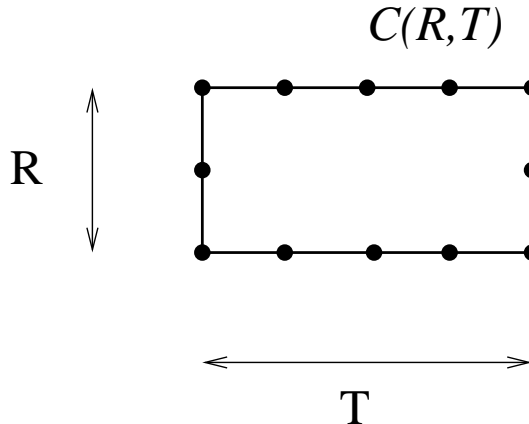


Figure 4: The construction of the  $R \times T$  wilson loop in a space-time plane.

though the calculations span a factor of two in lattice spacing  $a$ , from about 0.05 fm to 0.1 fm.

Do we expect the same picture of a rising, linear static-quark potential in full QCD, with dynamical quarks? As the two heavy quarks are separated, the energy stored in the string increases. Eventually, the string can “break” to form a quark-antiquark pair, a process that does not occur in the pure-gauge theory. This should lead to a flattening of the potential at some distance corresponding to an energy in the flux tube of  $2M_B$ , twice the binding energy of static-heavy-light meson. In practice, there has been no clear observation of such a feature at zero temperature from the simple Wilson loop operator; the behaviour of the potential in full QCD from a calculation using an  $\mathcal{O}(a)$ -improved fermion action<sup>21</sup> is shown in Figure 6.

As the string breaks, the  $Q\bar{Q}$  system crosses to a system of two heavy-light  $\bar{Q}q$  mesons. The lack of observation of the string breaking from the Wilson loop is ascribed to the poor overlap of the Wilson loop operator with two such heavy-light mesons. The mixing between these two states has been successfully investigated in simpler systems<sup>22,23,24</sup>, and recently a study has been made within QCD.<sup>25</sup> Both the ground state and first excited state energies are extracted by a variational calculation using the Wilson loop and  $Q\bar{q}\bar{Q}q$  operators, as shown in Figure 7. We will study a related problem when we discuss the nucleon-nucleon interaction in Section 4.

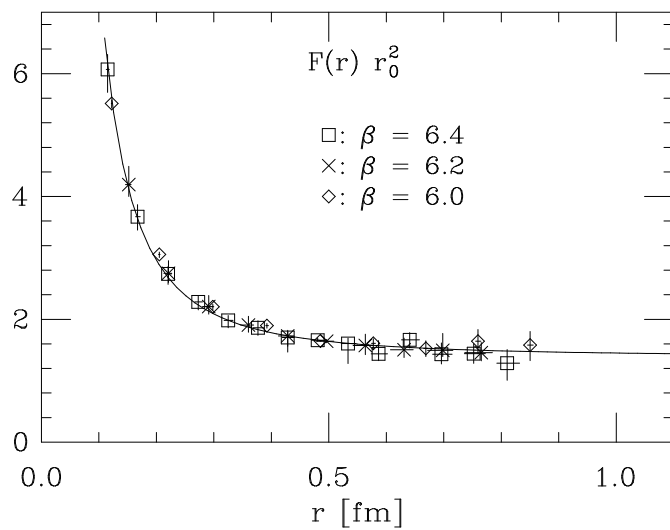


Figure 5: The force between two static quarks, in units of Sommer's  $r_0$  parameter,<sup>19</sup> is shown at three values of the lattice spacing, corresponding to  $\beta = 6.0, 6.2$  and  $6.4$ .<sup>20</sup>

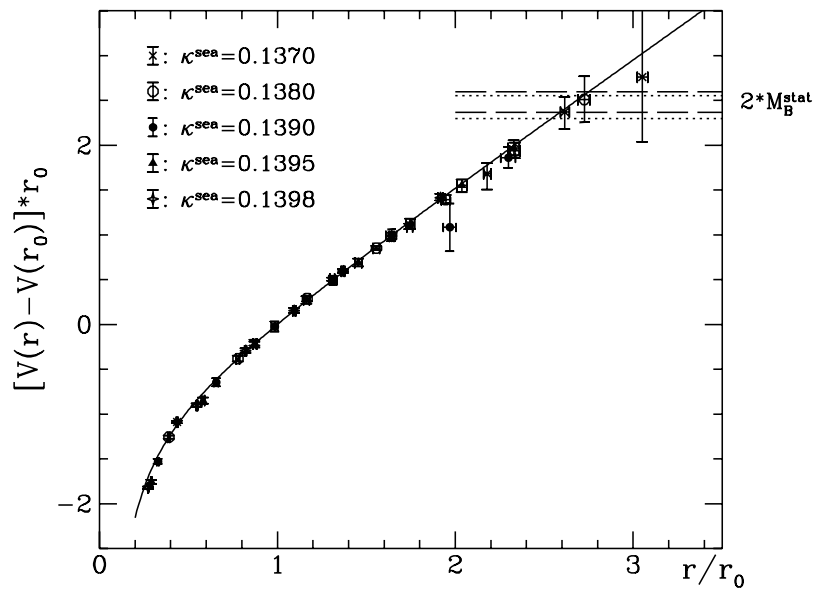


Figure 6: The scaled and normalised potential as a function of  $r/r_0$ , where  $r_0$  is the Sommer scale discussed earlier, as obtained on a  $12^3 \times 24$  lattice, using  $\mathcal{O}(a)$ -improved dynamical fermions.<sup>21</sup> The expected region of string breaking is shown by the horizontal lines.

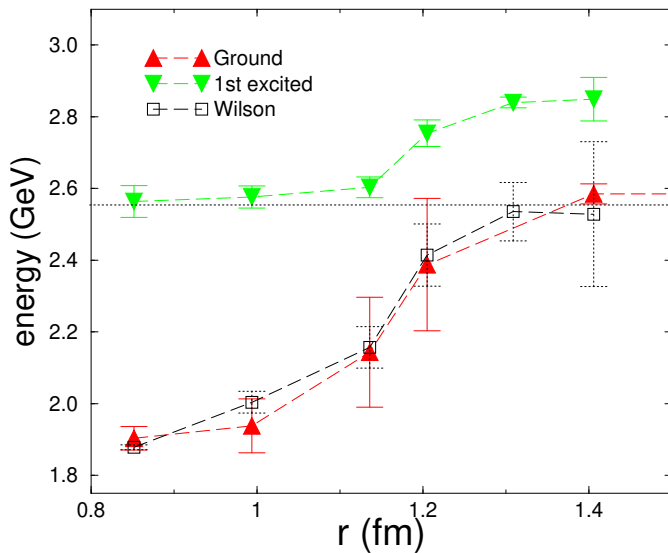


Figure 7: The ground and excited state energies obtained from a variational calculation including the  $Q\bar{Q}$  and  $Q\bar{q}\bar{Q}q$  operators.<sup>25</sup> The horizontal line is  $2M_B$ , the static binding energy shown also in Figure 6

## 2.2 Spectrum recipe

The elemental building blocks of a spectrum calculation are the quark propagators

$$G_{\alpha\beta}^{ij}(x, y) = \langle 0 | \psi_\alpha^i(x) \bar{\psi}_\beta^j(y) | 0 \rangle. \quad (36)$$

The quark propagator to every point  $x$  on the lattice from a *fixed* source point  $y$ , or linear combination of source points, is obtained by inverting the fermion matrix for a fixed source vector. There are a variety of linear-solver methods used to accomplish this.

In principle, the recipe for determining the mass of a ground-state hadron  $P$  is straightforward:

1. Choose an interpolating operator  $\mathcal{O}$  that has a good overlap with  $P$

$$\langle 0 | \mathcal{O} | P \rangle \neq 0,$$

and ideally a small overlap with other states having the same quantum numbers.

2. Form the time-sliced correlation function

$$C(t) = \sum_{\vec{x}} \langle \mathcal{O}(\vec{x}, t) \mathcal{O}^\dagger(\vec{0}, 0) \rangle.$$

This is expressed using a Wick expansion in terms of the quark propagators of Eq. 36

3. Insert a complete set of states between  $\mathcal{O}$  and  $\mathcal{O}^\dagger$ . The time-sliced sum puts the intermediate states at rest, and we find

$$\begin{aligned} C(t) &= \sum_{\vec{x}} \sum_P \int \frac{d^3 k}{(2\pi)^3 2E(\vec{k})} \langle 0 | \mathcal{O}(\vec{x}, t) | P(\vec{k}) \rangle \langle P(\vec{k}) | \mathcal{O}^\dagger(\vec{0}, 0) | 0 \rangle \\ &= \sum_P \frac{|\langle 0 | \mathcal{O} | P \rangle|^2}{2 M_P} e^{i M_P t}. \end{aligned}$$

4. Continue to Euclidean space  $t \rightarrow it$ , and we find

$$C(t) = \sum_P \frac{|\langle 0 | \mathcal{O} | P \rangle|^2}{2 M_P} e^{-M_P t}. \quad (37)$$

At large times, the lightest state dominates the spectral sum in Eq. (37), and we can extract the ground state mass.

However there are many considerations that complicate this picture. Firstly, the temporal separation between the hadrons must be sufficiently large that the ground state can be identified in Eq. (37); we aim to accomplish this by choosing an operator having a large overlap with the ground state relative to the excited states, and by fitting to several interpolating operators. Secondly, the correlation lengths in our calculation must be small compared with the size of the box in which we are working. This correlation length is simply the inverse of the pion mass, and we require  $m_\pi L \simeq 5$ , where  $L$  is the spatial extent of the lattice. Most, though not all, simulations to date have restricted consideration to quark masses in the region of the strange-quark mass.

The benchmark calculation of the quenched light-hadron spectrum using the unimproved fermion action has been performed by the CP-PACS collaboration.<sup>26</sup> They perform their calculation on a variety of lattice sizes, to control finite size effects, and at a variety of lattice spacings, to enable an extrapolation to the continuum limit.

Recently, there has been a similar calculation using the non-perturbatively improved clover fermion action by the UKQCD Collaboration.<sup>27</sup> They also perform an extrapolation to the continuum limit, but in their case the discretisation uncertainties are  $\mathcal{O}(a)$  rather than  $\mathcal{O}(a^2)$ , and I will describe some of the details of this calculation.

UKQCD generated  $16^3 \times 32$  lattices at  $\beta = 5.7$ ,  $16^3 \times 48$  lattices at  $\beta = 6.0$  and  $24^3 \times 48$  lattices at  $\beta = 6.2$ , corresponding to approximately a factor two span of lattice spacings but at roughly the same spatial volumes. In addition, a calculation was performed on a larger  $32^3 \times 64$  lattice at  $\beta = 6.0$  to enable a study of finite-volume effects. Quark propagators were computed with the clover coefficient having both its tadpole-improved value  $c_{\text{SW}} = \text{TAD}$  ( $\beta = 5.7, 6.0, 6.2$ ), and its non-perturbatively determined value  $c_{\text{SW}} = \text{NP}$  ( $\beta = 6.0, 6.2$ ).

Since the quark propagators were computed at values of the quark mass in the region of the strange quark mass, it is necessary to extrapolate in the quark mass to obtain results at the  $u$ - and  $d$ -quark masses, and interpolate to obtain results at the  $s$ -quark mass. The bare, or unrenormalised quark mass, is related to the hopping parameter  $\kappa$  through

$$m_q = \frac{1}{2a} \left( \frac{1}{\kappa} - \frac{1}{\kappa_{\text{crit}}} \right). \quad (38)$$

The bare quark mass must be rescaled in the  $\mathcal{O}(a)$ -improved theory so that

spectral quantities approach the continuum limit with  $\mathcal{O}(a^2)$ ,<sup>17</sup>

$$\tilde{m}_q = m_1(1 + b_m a m_q), \quad (39)$$

where the perturbative one-loop value of  $b_m$  is used.<sup>28</sup> To extrapolate the results to the physical quark masses, the following ansatz is employed:

$$m_{\text{PS}}^2 = B(\tilde{m}_{q,1} + \tilde{m}_{q,2}) \quad (40)$$

$$m_{\text{V}} = A_{\text{V}} + C_{\text{V}}(\tilde{m}_{q,1} + \tilde{m}_{q,2}) \quad (41)$$

$$m_{\text{Oct}} = A_{\text{Oct}} + C_{\text{Oct}}(\tilde{m}_{q,1} + \tilde{m}_{q,2} + \tilde{m}_{q,3}) \quad (42)$$

$$m_{\text{Dec}} = A_{\text{Dec}} + C_{\text{Dec}}(\tilde{m}_{q,1} + \tilde{m}_{q,2} + \tilde{m}_{q,3}), \quad (43)$$

where the subscripts PS, V, Oct and Dec refer to the pseudoscalar meson, vector meson, octet baryons ( $\Sigma$ - and  $\Lambda$ -like) and decuplet baryons ( $\Delta$ -like) respectively. The critical hopping parameter corresponds to the value of  $\kappa$  for which  $m_{\text{PS}}$  vanishes. The quality of the chiral extrapolations of the vector,  $\Sigma$  and  $\Lambda$  masses for the  $c_{\text{SW}} = \text{NP}$  data is shown in Figure 8.

The  $c_{\text{SW}} = \text{TAD}$  data has in principle a remnant  $\mathcal{O}(a)$  discretisation error, whilst the  $c_{\text{SW}} = \text{NP}$  data is fully  $\mathcal{O}(a^2)$ -improved. In the continuum extrapolations, UKQCD performs a simultaneous fit to both the NP and TAD data. In order to investigate the approach to the continuum limit, it is not necessary to study the chirally extrapolated values. Indeed, a clear demonstration of the efficacy of improvement can be seen by looking at the lattice-spacing dependence of hadron masses at a fixed  $m_\pi/m_\rho$  ratio,<sup>29</sup> shown in Figure 9.

The final UKQCD results for the quenched light-hadron spectrum, together with the CP-PACS results using the standard Wilson fermion action, are shown in Figure 10. The different UKQCD plotting symbols correspond to determining the lattice spacing by requiring that either  $K^*$  or  $N$  have its physical value. Both calculations support the assertion that the quenched light-hadron spectrum agrees with experiment at the 10% level. Now that we have established the reliability with which we can compute the known hadron masses, it is time to investigate the predictive power of lattice QCD. We begin by considering the glueball spectrum.

### 2.3 Glueball Spectrum

The gluon self-coupling that distinguishes QCD from the Abelian QED admits the existence of purely gluonic bound states, or glueballs. Indeed, glueballs are the only true states in quenched QCD! The good agreement of the quenched light-hadron spectrum with the experimental value was perhaps not surprising; Zweig's rule tells us that hadronic decays involving the annihilation of the

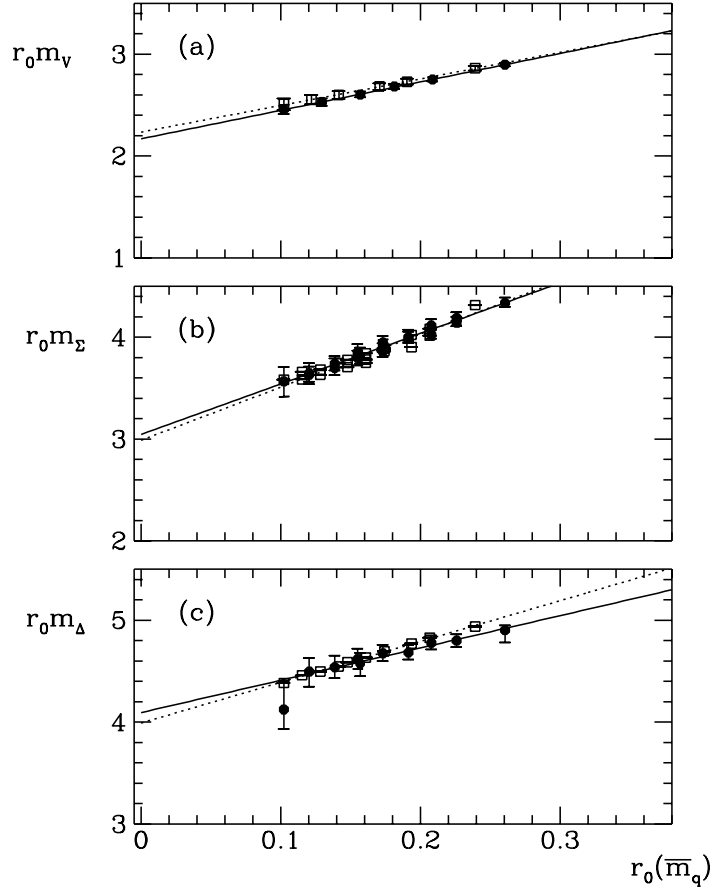


Figure 8: Data<sup>27</sup> for (a): vector mesons, (b):  $\Sigma$ -like baryons and (c):  $\Delta$ -like baryons is plotted against the average value of the masses of the component quarks  $\bar{m}_q = (\tilde{m}_{q,1} + \tilde{m}_{q,2})/2$  (vector meson) and  $\bar{m}_q = (\tilde{m}_{q,1} + \tilde{m}_{q,2} + \tilde{m}_{q,3})/3$  (baryons). Squares and circles denote the NP data at  $\beta = 6.2$  and  $\beta = 6.0$  respectively, and the lines correspond to the fits of Eqs. (41)-(43)

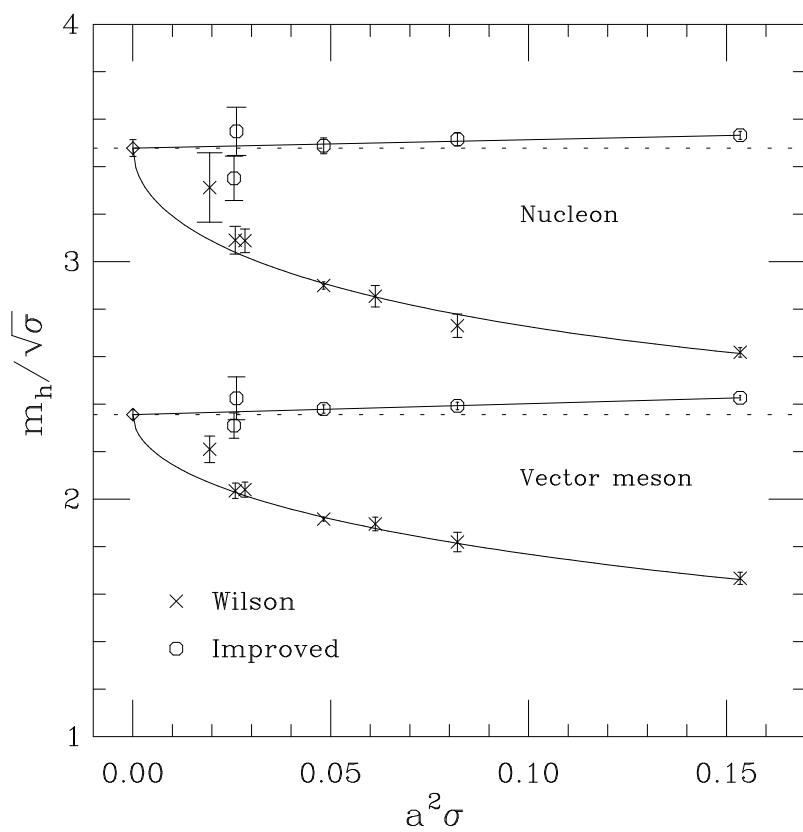


Figure 9: The hadron spectrum using the Wilson and non-perturbatively improved fermion actions is shown against  $a^2$  at fixed  $m_{PS}/m_V$ .<sup>29</sup> The scale is set from the string tension.

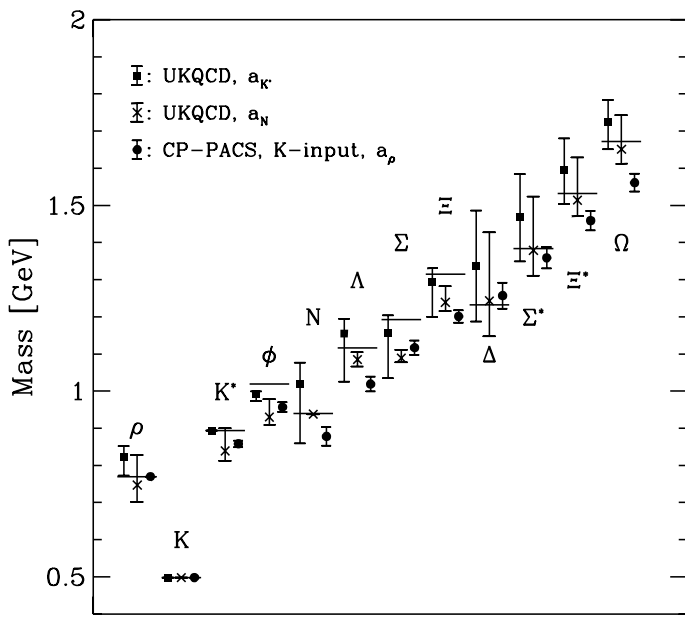


Figure 10: The quenched light hadron spectrum computed in the  $\mathcal{O}(a)$ -improved theory<sup>27</sup> and the comparison to results obtained using the unimproved Wilson action (full circles).<sup>26</sup> The levels of the experimental points are denoted by solid lines

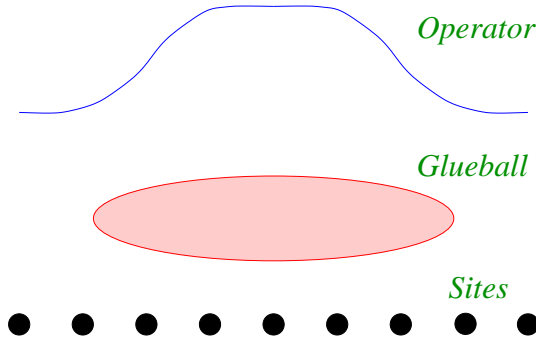


Figure 11: Construction of improved glueball operators, with the aim of increasing the overlap with the ground state.

initial quarks are highly suppressed. Zweig's rule also suggests that glueball mixing with quark states should be similarly suppressed. Thus a quenched calculation of the glueball spectrum is very important, and can yield crucial information to guide experiment.

The calculation of the glueball spectrum has been plagued by two inter-related problems. Firstly, the glueballs are relatively heavy and thus the correlation functions die rapidly at increasing temporal separations. Secondly the glueball correlators are subject to large fluctuations independent of separation. In consequence, the signal-to-noise ratio for glueball correlators is very poor.

Calculations of the spectrum using the standard Wilson gluon action, Eq. (11), have emphasised the construction of improved gluonic operators which more correctly describe the ground-state glueball wave function, as illustrated in Figure 11. In the case of the determination of the spectrum of states at rest, the rotation group used in the construction of the continuum glueball operators is reduced to the cubic group of the lattice. The different components of, for example, the  $J^{PC} = 2^{++}$  glueball lie in the  $E^{++}$  and  $T_2^{++}$  representations of the cubic group. As the continuum limit is approached, the masses obtained from the different representations of the cubic group should become degenerate, signifying the restoration of rotation symmetry. Despite the discretisation errors of the standard Wilson gauge action being  $\mathcal{O}(a^2)$ , the lightest glueball state is subject to much larger  $\mathcal{O}(a^2)$  discretisation errors than the spectrum for quark states, as shown in Figure 12.<sup>30</sup>

To improve upon these calculations, Morningstar and Peardon<sup>31</sup> chose to employ an  $\mathcal{O}(a^2)$ -improved gluon action, having discretisation errors of

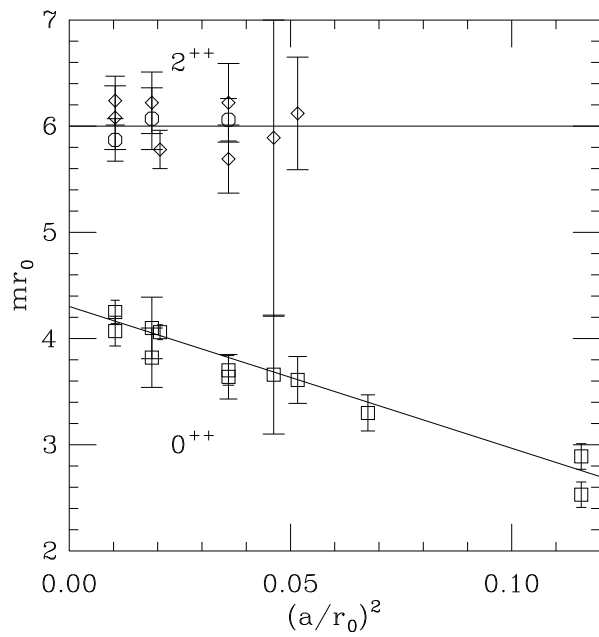


Figure 12: The continuum extrapolation of the masses of the  $J^{PC} = 0^{++}$  and  $2^{++}$  states.<sup>30</sup> The different plotting symbols for the  $2^{++}$  states correspond to the lattice operators  $T_2$  (octagons) and  $E$  (diamonds). The lines represent linear continuum extrapolations in  $a^2$ .

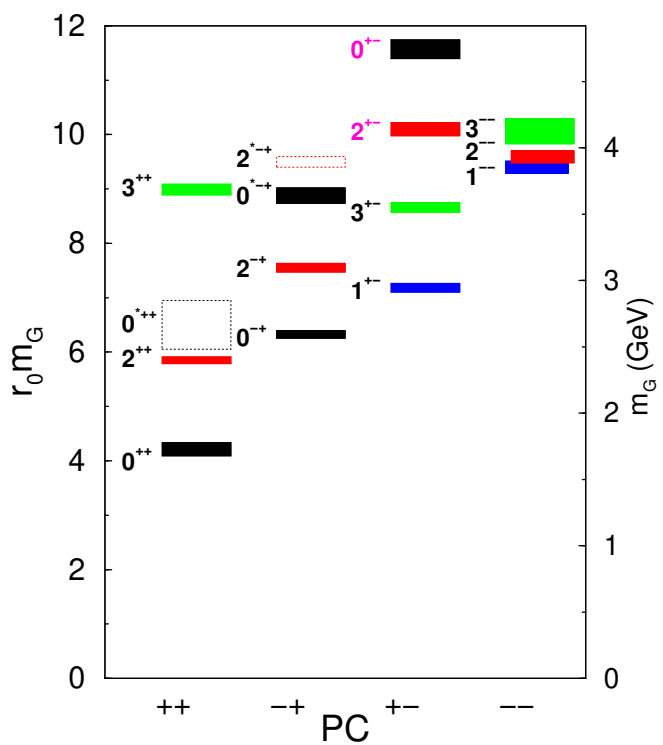


Figure 13: The quenched glueball spectrum is shown after extrapolation to the continuum limit.<sup>33</sup>

$\mathcal{O}(a^4)$ ; note that it is only necessary to consider operators of even dimension in the construction of the gluonic part of the action. Unfortunately, the relatively large mass of the glueball states in lattice units allows only a couple of time slices to be used in extracting the glueball masses. They then observed that one could employ a relatively coarse lattice in the spatial directions to produce a reasonable approximation to the glueball wave function, whilst employing a finer lattice in the temporal direction to enable the isolation of the ground state and excited state masses in each channel.<sup>32</sup>

The anisotropic lattice is implemented through the choice of different coupling constants for the space-space and space-time plaquettes in the gluonic action Eq. 11; this involves a non-trivial tuning, since the bare couplings are renormalised. The resulting glueball spectrum<sup>33</sup> after extrapolation to the continuum limit, is shown in Figure 13.

#### 2.4 Exotic Hadrons

The search for hadrons with excited glue is one of the primary goals of the  $N^*$  programme at CEBAF. There has been a flurry of recent activity looking for exotic states, and in particular exotic mesons, in the lattice community; lattice gauge theory aficionados generally try to comprehensively understand the mesonic sector before venturing into the realm of baryons.

#### Exotics and Hybrids

Within the quark model, the charge conjugation  $C$  and parity  $P$  of a meson are related to the spin  $S$  and orbital angular momentum  $L$  through

$$P = (-1)^{L+1}; C = (-1)^{L+S}.$$

States not conforming to these relations are called exotics, and examples are the states with

$$J^{PC} = 1^{-+}, 0^{+-}, 2^{+-}.$$

An exotic can be formed in two ways. Firstly, as a quark-antiquark-glue state, which we call a hybrid. Secondly as a bound state of two quarks and two antiquarks. In this section I will discuss lattice studies of hybrid states. These studies have been given increased impetus by experimental observations of  $1^{-+}$  resonance states in the region of 1.4 GeV.<sup>34,35</sup>

#### Hybrid interpolating operators

The usual interpolating operator for the pion is

$$\mathcal{O}_\pi(\vec{x}, t) = \bar{\psi}(\vec{x}, t) \gamma_5 \psi(\vec{x}, t). \quad (44)$$

In the case of the hybrid state  $1^{-+}$ , a possible interpolating operator would be

$$\mathcal{O}_{1-+}(\vec{x}, t) = \bar{\psi}(\vec{x}, t) \gamma_i F_{ij}(\vec{x}, t) \psi(\vec{x}, t) \quad (45)$$

where  $F_{ij}$  is a lattice discretisation of the field-strength tensor constructed in Figure 3. In practice to get any sort of signal for hybrid mesons, it is necessary to use interpolating operators in which the quark and antiquark are separated in space. The signals are inevitably much noisier than for the pseudoscalar and vector meson states. To see why, we note that the hybrid correlator  $C_{\text{hyb}}(t)$  decays exponentially with the mass of the hybrid,

$$C_{\text{hyb}}(t) \simeq e^{-m_{\text{hyb}} t}. \quad (46)$$

In contrast, the correlator for the variance is that of the square of the interpolating operator

$$C_{\sigma^2}(t) = \sum_{\vec{x}} \langle |\mathcal{O}_{\text{hyb}}(\vec{x}, t)|^2 |\mathcal{O}_{\text{hyb}}(\vec{0}, 0)|^2 \rangle. \quad (47)$$

Typically,  $|\mathcal{O}_{\text{hyb}}|^2$  is an interpolating operator for two pions, and therefore the signal-to-noise ratio with increasing temporal separations increases as

$$\frac{\text{signal}}{\text{noise}} \simeq e^{-(m_{\text{hyb}} - m_{\pi})t}. \quad (48)$$

Since the masses of the hybrids are relatively large, the signal quickly is lost in the noise. In the case of the glueball calculations, the situation is particularly severe since the square of the glueball operator has a non-zero vacuum expectation value, leading to the constant noise alluded to earlier.

There have been recent calculations of the light-quark hybrid spectrum, and in particular of the  $1^{-+}$  state, in both the quenched approximation<sup>36,37</sup> and in full QCD<sup>38,39</sup>. Indeed, there has even been a measurement of the Coulomb-gauge wave function for the  $1^{-+}$  state, shown in Figure 14, in which the separation between the quark and anti-quark is clearly apparent. These calculations all find a  $1^{-+}$  mass around 2 GeV, far larger than that of the experimental candidates. A possible resolution is that this resonance is actually a four-quark state; we will return to this interpretation in Section 4.

## 2.5 The $N^*$ Spectrum

The measurement of the excited nucleon spectrum reveals the full  $SU(3)$  nature of QCD, and is a critical part of the experimental programme at CEBAF. The observed  $N^*$  spectrum is shown schematically in Figure 15. The nu-

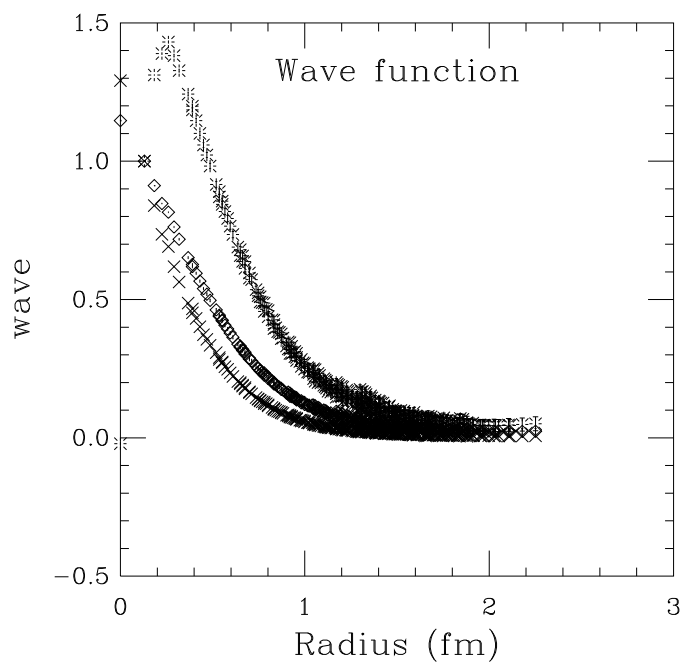


Figure 14: The wave function in Coulomb gauge of the  $\pi$  (crosses),  $\rho$  (diamonds) and  $1^{-+}$  state (bursts) obtained from quenched QCD at  $\beta = 5.85^{37}$

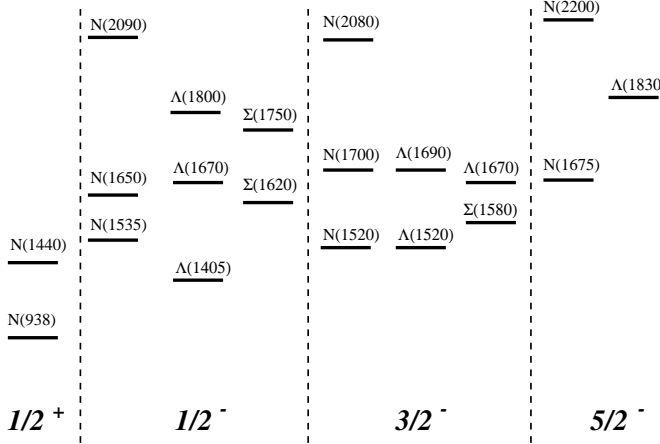


Figure 15: Schematic showing the observed  $N^*$  spectrum, labelled by  $J^P$ .

cleon  $N(938)$  has positive parity; its parity partner, with negative parity, is the  $N(1535)$ . The usual nucleon interpolating operators employed in lattice calculations are

$$N_\alpha = \epsilon^{ijk} (u^i C \gamma_5 d^j) u_\alpha^k. \quad (49)$$

On forming the time-sliced correlator, both positive and negative parity states can contribute to the correlation function. However, we can perform a parity projection

$$C(t) = \sum_{\vec{x}} \langle 0 | N_\alpha(\vec{x}, t) (1 \pm \gamma_0)_{\alpha\beta} \bar{N}_\beta(0) | 0 \rangle \quad (50)$$

to project out the forward-propagating positive (+ sign) or negative (- sign) parity states, with states of the opposite parity propagating in the negative direction. On a periodic lattice, our correlator contains both the forward- and backward-propagating states, and we rely on a sufficiently long temporal extent to our lattice to delineate the two parities.

Recently, there have been two lattice calculation of this mass splitting. The first<sup>40</sup> employs a highly improved fermion action, the  $D_\chi 34$  action of Hamber and Wu.<sup>41</sup> Not only do the authors extract the mass of the  $J = 1/2^-$  state, but also find a signal for the  $J = 3/2^-$  state. The second calculation<sup>42</sup> employs domain-wall fermions; here the authors argue that, since the  $J = 1/2^+$  and  $J = 1/2^-$  state are degenerate in an unbroken chirally symmetric theory, the

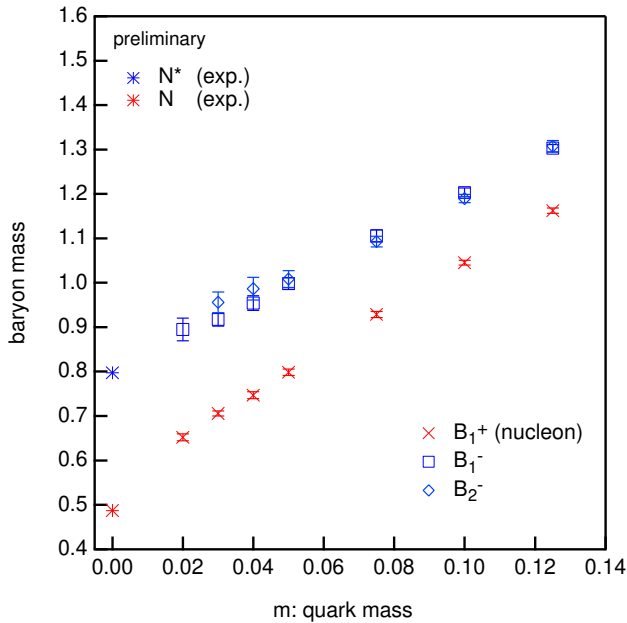


Figure 16: The masses of the nucleon (N) and its negative-parity partner in lattice units ( $a^{-1} \simeq 1.9$  GeV using the  $\rho$  mass to set the scale).<sup>42</sup>

use of an action having a possessing exact chiral symmetry, even at non-zero lattice spacing, is crucial in correctly extracting the splitting.

Both calculations find mass splittings between the positive- and negative-parity states in accord with experiment, though with still substantial systematic and statistical uncertainties. The masses of the  $J = 1/2^+$  (nucleon) and  $J = 1/2^-$  states using DWF at a fixed value of the lattice spacing are shown in Figure 16.

### 3 Hadron Structure

As well as enabling the calculation of the hadron spectrum, lattice QCD enables the study of the distribution of the quarks and gluons within hadrons. Information about these is contained in the form factors, and in the quark and gluon structure functions. These calculations have in common the determination of some (local) hadronic matrix element, so we will begin this section with

a discussion of the lattice technology of determining matrix elements.

### 3.1 Hadronic Matrix Elements

The paradigm calculation is that of  $f_\pi$ , the pion decay constant defined through

$$\langle 0 | A_\mu | \pi \rangle = i p_\mu f_\pi, \quad (51)$$

where  $A_\mu \equiv \bar{\psi} \gamma_\mu \gamma_5 \psi$  is the axial vector current. This matrix element we can obtain as a by-product of the determination of  $m_\pi$ , and our analysis will follow that of Section 2.2. We construct the correlator

$$C(t) = \sum_{\vec{x}} \langle 0 | A_4^{\text{lat}}(\vec{x}, t) A_4^{\text{lat}}(0) | 0 \rangle, \quad (52)$$

where  $A^{\text{lat}}$  is a lattice discretisation of the continuum axial-vector current. Inserting a complete set of states between the two interpolating operators, we obtain

$$\begin{aligned} C(t) &= \sum_{\vec{x}} \sum_P \frac{1}{(2\pi)^3} \int \frac{d^3 \vec{p}}{2E(\vec{p})} \langle 0 | A_4^{\text{lat}}(\vec{x}, t) | P(\vec{p}) \rangle \langle P(\vec{p}) | A_4^{\text{lat}\dagger}(0) | 0 \rangle \\ &= \sum_{\vec{x}} \sum_P \frac{1}{(2\pi)^3} \int \frac{d^3 \vec{p}}{2E(\vec{p})} e^{-iEt + i\vec{p} \cdot \vec{x}} \langle 0 | A_4^{\text{lat}}(0) | P(\vec{p}) \rangle \langle P(\vec{p}) | A_4^{\text{lat}\dagger}(0) | 0 \rangle \\ &= \sum_P \int \frac{d^3 \vec{p}}{2E(\vec{p})} e^{-iEt} \delta^{(3)}(\vec{p}) \langle 0 | A_4^{\text{lat}} | P(\vec{p}) \rangle \langle P(\vec{p}) | A_4^{\text{lat}\dagger} | 0 \rangle \\ &\xrightarrow{t \rightarrow \infty} \frac{1}{2} m_\pi f_\pi^{\text{lat}2} e^{-m_\pi t} + \text{excited states} \end{aligned} \quad (53)$$

The lattice discretisation has provided both a cut-off, and a renormalisation scheme. We, of course, want  $f_\pi$  in some familiar continuum scheme, such as  $\overline{\text{MS}}$ . To provide us with that, we need to compute the matching coefficient  $Z_A$  for the axial vector current, such that

$$A_\mu^R = Z_A A^{\text{lat}}. \quad (54)$$

The determination of the matching coefficient  $Z$  is one of the most delicate, and generally onerous, tasks of any calculation of hadronic matrix elements. The lattice formulation reproduces continuum QCD as the lattice spacing approaches zero, and thus the anomalous dimensions of the operators in the lattice formulation matches those of the continuum operators. However, the replacement of the continuum Lorentz symmetry by the hypercubic symmetry

of the lattice, and the lack of chiral symmetry in most fermion formulations, complicates the calculation of the matching coefficients enormously, even for such a simple operator as the axial vector current. In particular, the lattice allows mixing with higher dimension operators, combined with appropriate powers of the lattice spacing  $a$ . An important element of the improvement programme is finding a combination of lattice operators such that matrix elements are free of  $\mathcal{O}(a)$ , or higher, discretisation errors.

In principle, we can compute  $Z$  in perturbation theory. Perturbation theory using the bare lattice coupling  $g$  as an expansion parameter apparently fails, resulting in very large perturbative corrections. The bulk of these large corrections can be identified as lattice artifacts, the “tadpole” contributions arising from the  $\mathcal{O}(g^2)$  term in the expansion of the link variable, Eq. 8. These terms can effectively be resummed through the expansion in terms of a renormalised coupling constant.<sup>15</sup> This prescription is precisely that used in the specification of the tadpole-improved clover coefficient of Eq. 30.

An alternative route is to attempt to determine the matching coefficients, and improvement coefficients, non-perturbatively through the imposition of chiral Ward identities.<sup>16</sup> Indeed, this prescription enables, in principle, the elimination of all  $\mathcal{O}(a)$  discretisation effects from on-shell quantities, providing appropriate renormalisation conditions can be found.

Both these routes require considerable effort, and uncertainty in the calculation of matching and improvement coefficients is a major uncertainty in the calculation of hadronic matrix elements. Let me conclude this subsection by noting that the chiral fermion actions of Section 1.6 are automatically  $\mathcal{O}(a)$ -improved, and admit a smaller degree of operator mixing. This may be prove a substantial advantage for these formulations.

### 3.2 Nucleon Form Factors

The electric and magnetic form factors of the nucleon are among the simplest quantities that contain information about the structure of the nucleon, and are measured in electron proton scattering. They are related to the matrix elements of the vector current  $J_\mu$  through

$$\langle p', s' | J_\mu(q) | p, s \rangle = \bar{u}(p', s') \left[ \gamma_\mu F_1(q^2) + i\sigma_{\mu\nu} \frac{q^\nu}{2m_N} F_2(q^2) \right] u_p(p, s), \quad (55)$$

where  $q = p - p'$  is the momentum of the photon probe. Note that  $F_1$  and  $F_2$  satisfy

$$F_1(0) = 1; \quad F_2(0) = \mu - 1$$

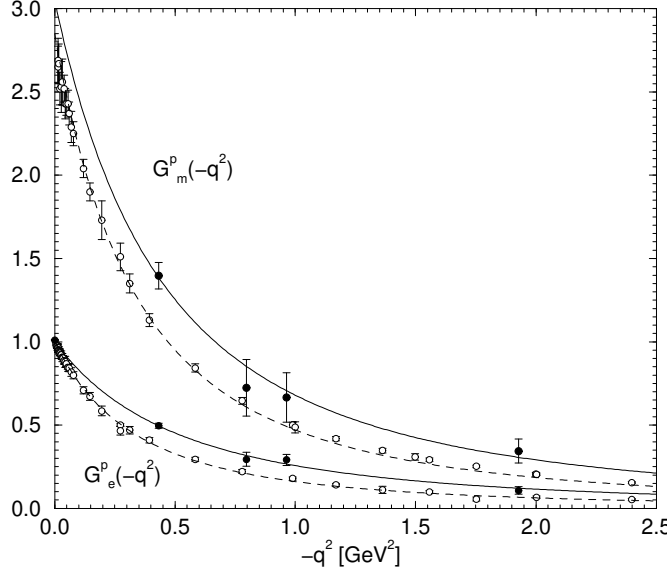


Figure 17: The solid points are lattice determinations of the electric and magnetic form factors of the proton in the quenched approximation to QCD.<sup>43</sup> The open circles are the experimental measurements.<sup>44</sup> The lines represent the dipole fits of Eq. 58 to the experimental and lattice data.

where the former result expresses current conservation, and  $\mu$  is the magnetic moment of the nucleon. For point-like particles, both quantities would be constant, and therefore they are a measure of the spatial extent of the nucleon. Rather than quoting these quantities directly, it is usual to form the Sach's form factors

$$G_E(q^2) = F_1(q^2) + \frac{q^2}{4m_N^2} F_2(q^2) \quad (56)$$

$$G_M(q^2) = F_1(q^2) + F_2(q^2), \quad (57)$$

where we note that  $q^2$  is space-like.

Phenomenologically, it is usual to parameterise the form factors through the vector dominance model by a dipole fit

$$G_E^p(q^2) \sim G_M^p(q^2)/\mu^2 \sim G_M^N(q^2) \sim \frac{1}{(1 - q^2/m_V^2)^2}$$

$$G_E^n(q^2) \sim 0. \quad (58)$$

A recent lattice determination of the proton electromagnetic form factors<sup>43</sup> is shown in Figure 3.2, together with the experimental data.<sup>44</sup> The lines are fits to the data using the dipole forms of Eq. 58.

### 3.3 Hadronic Structure Functions

The hadronic structure functions, describing the distribution of quarks and gluons inside, say, a nucleon in inclusive processes, are related to the hadronic tensor

$$W_{\mu\nu} = \frac{1}{4\pi} \int d^4x e^{iq\cdot x} \langle N(p, s) | J_\mu(x) J_\nu(0) | N(p, s) \rangle, \quad (59)$$

where  $J_\mu$  is the electroweak current, and  $p, s$  are the nucleon momentum and spin respectively. Decomposing  $W_{\mu\nu}$  according to the possible Lorentz structures yields four structure functions, two spin-averaged,  $F_{1,2}(x, Q^2)$  and two spin-dependent,  $g_{1,2}(x, Q^2)$ , where  $x$  is the Bjorken variable, and  $Q^2 = -q^2$ . Phenomenologically, these are determined in Deep Inelastic Scattering, and parameterised at some reference energy scale.

Near the light cone,  $x^2 \sim 0$ , the structure functions can be expanded using the operator product expansion (OPE) in terms of the matrix elements of certain local operators, of twist (dimension - spin) two, together with Wilson coefficients calculable in perturbation theory. Historically, it is these matrix elements that are computed in lattice simulations, since the non-zero lattice spacing in our calculations precludes the measurement of the currents in Eq. 59 at sufficiently small separations, and more fundamentally it is unclear how to extract this quantity at light-like separations in Euclidean space.

The local matrix elements are related to the  $x$ -moments of the structure functions. In principle, we can recover the full  $x$ -dependence of the structure functions by measuring increasing moments. The simplest operators are the non-singlet operators for both the unpolarised and polarised structure functions,

$$\begin{aligned} \mathcal{O}_{\mu_0 \dots \mu_n} &= \bar{\psi} \gamma_{\mu_0} iD_{\mu_1} \dots iD_{\mu_n} \tau \psi \\ \mathcal{O}_{\mu_0 \dots \mu_n}^5 &= \bar{\psi} \gamma_5 \gamma_{\mu_0} iD_{\mu_1} \dots iD_{\mu_n} \tau \psi, \end{aligned} \quad (60)$$

where symmetrisation of indices and removal of traces is understood, and the  $\tau$  is an SU(2) flavour matrix. The first few moments moments for the nucleon have been measured by several groups.<sup>46,47,49,50</sup>

The lowest moment of the unpolarised quark distribution has a particularly simple interpretation in terms of the momentum fraction carried by the quarks.

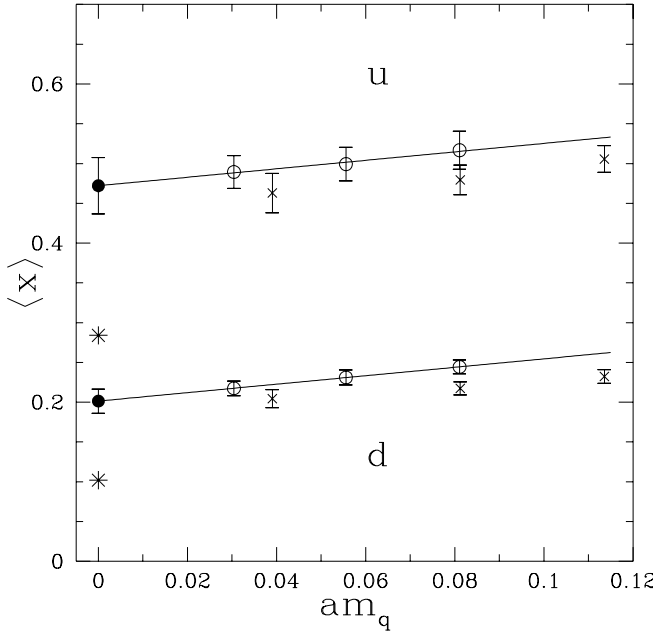


Figure 18: The first moment of the unpolarised  $u$  and  $d$  quark distributions in the nucleon as a function of the quark mass at  $\beta = 6.0$ <sup>51</sup>. The circles and crosses denote results with the Wilson and clover fermion actions respectively. The bursts denote the CTEQ results.<sup>48</sup>

Figure 18 shows the first moment of the  $u$  and  $d$  quark distributions in the quenched approximation,<sup>51</sup> both distributions are somewhat higher than phenomenological expectations. Unfortunately, it is unclear the extent to which the calculation of the first few moments of the structure functions enables a useful picture of the  $x$ -dependence of the structure functions, and a means of performing a direct computation of the hadronic tensor, Eq. 59, would be invaluable.

The study of the flavour-singlet sector involves consideration of both the quark and gluon distributions, which mix. Computationally, these studies are much more demanding, but of tremendous interest since they venture beyond the simple valence picture of the nucleon. More recently, there have been attempts to investigate the rôle of higher-twist contributions,<sup>52</sup> to which upcoming experiments at JLAB should be particularly sensitive.

## 4 The Nucleon-Nucleon Interaction

In the preceding, we have used lattice gauge theory to acquire a fundamental understanding of the internal structure of an isolated hadron from first principles. It is natural to aim at a similar understanding of the interactions between hadrons, and in particular of the nucleon-nucleon interaction, the very foundation of nuclear physics.

Understanding the strong interaction in multi-hadron systems from lattice QCD is a notoriously difficult problem. Multi-hadron states involve the computation of a four-point function and are relatively massive, and therefore the corresponding correlation functions quickly vanish into noise at increasing temporal separations. Furthermore, multi-hadron systems are large, and therefore the spatial extent of the lattice needs to be correspondingly larger than that used in hadronic spectroscopy. Finally, the use of a Euclidean lattice obscures the extraction of the phase information of the full scattering matrix.<sup>45</sup> Despite these difficulties, the problem is fundamental and compelling.

Historically, there have been two approaches to this problem within lattice QCD. The first aimed to extract certain quantitative parameters of the hadron-hadron interaction by direct lattice simulation. Lüscher<sup>53,54,55</sup> exploited the finite-size dependence to extract a discrete set of  $s$ -wave scattering lengths. This was thoroughly tested within an  $O(4)$ -symmetric  $\phi^4$  model<sup>56</sup>, and scattering lengths have been computed within QCD for pions<sup>57,58</sup> and for nucleons.<sup>57</sup> Fiebig *et al.*<sup>59</sup> explored the  $I = 2$   $\pi - \pi$  system by extracting a residual interaction potential, and then proceeded to compute the scattering phase shifts which were compared with experiment.

The extraction of the  $s$ -wave scattering lengths of the  $\pi - \pi$  interaction has been encouraging, as illustrated in Figure 19 where the  $s$ -wave scattering length for the isospin  $I = 2$  pion-pion interaction is shown.<sup>58</sup> The investigation of the  $N - N$  system is more problematical. Here the scattering lengths are of the order of 10 fm, rather than less than 1 fm as is the case for the  $\pi - \pi$  interaction. Therefore, while lattice calculations do indeed find scattering lengths for the  $N - N$  interaction considerably larger than those for the  $\pi - \pi$  and  $\pi - N$  interaction,<sup>57</sup> this approach is limited by our present inability to simulate on lattice sizes of the order of 10–20 fm, and at physical values of the pseudoscalar mass.

The second approach is motivated by the realisation that important insight into the nucleon-nucleon interaction can be gleaned by studying the interactions of a much simpler system, that of two heavy-light mesons, with static heavy quarks.<sup>60,61</sup> Such a system exhibits most of the salient features of the nucleon-nucleon system, namely quark exchange, flavour exchange and colour

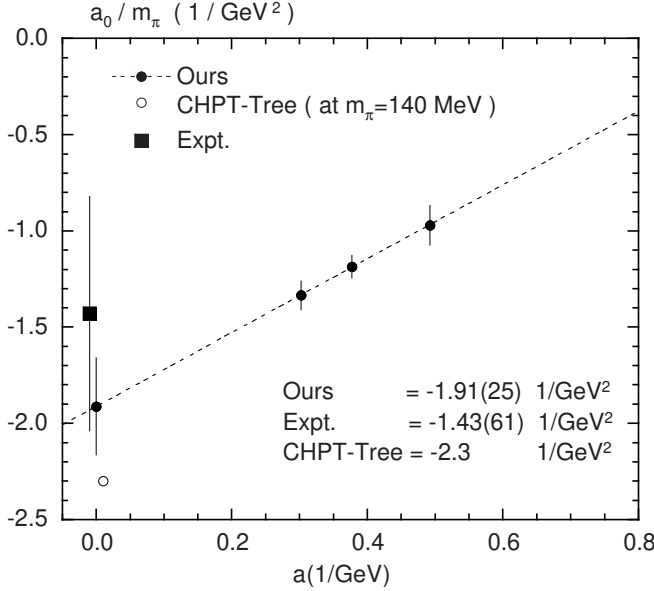


Figure 19: The  $I = 2$  pion scattering length obtained in the quenched approximation to QCD is shown as a function of the lattice spacing, and in the continuum limit.<sup>58</sup> Also shown as the open circle is the current-algebra prediction for  $m_\pi = 140$  MeV.

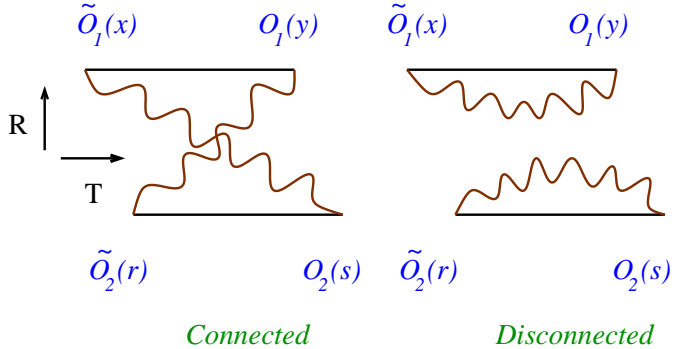


Figure 20: The connected (flavour-exchange) and disconnected contributions to the interaction between two heavy-light mesons are shown. The solid lines denote the heavy quarks, whilst the curly lines denote the propagation of the light-quarks.

polarization. The interaction between the mesons can be understood by the study of the four-point functions, shown in Figure 20:

$$C^{(4)}(x, r; y, s) = \langle O_1(y)O_2(s)\tilde{O}_1^\dagger(x)\tilde{O}_2^\dagger(r) \rangle. \quad (61)$$

Here each operator can either be that for a pseudoscalar ( $P$ ) or for a vector ( $V$ ). The range of the interaction can be assessed by forming the  $z$ - and  $t$ -sliced sum,

$$\tilde{C}(R, T) = \sum_{t_1, t_2, \vec{a}_\perp} C(x, r; y, s), \quad (62)$$

where

$$\begin{aligned} x &= (\vec{0}, t_1), y = (\vec{0}, t_1 + T) \\ r &= (\vec{a}_\perp, R, t_2), s = (\vec{a}_\perp, R, t_2 + T). \end{aligned}$$

At large distances  $R$  and times  $T$ , the correlation function is dominated by the lightest state  $|n\rangle$ , of mass  $M_n$ , that can be exchanged between the mesons, with

$$\tilde{C}(R, T) \sim e^{-M_n R} \langle 0 | O_1(\vec{0}, T) \tilde{O}_1^\dagger(\vec{0}, 0) | n \rangle \times \langle n | O_2(\vec{0}, T) \tilde{O}_2^\dagger(\vec{0}, 0) | 0 \rangle. \quad (63)$$

Can these correlation functions be constructed from the elemental quark propagators of Eq. 36? The connected diagram of Figure 20 requires the evaluation of the propagator from one point on every time slice to every point on the lattice; this is manageable. Unfortunately, the computation of the disconnected diagram requires the evaluation of all-to-all propagators. Nonetheless, the study of the connected diagram alone is valuable. It describes the flavour-exchange interaction, and lattice simulations have shown that the interaction is indeed mediated by meson exchange at large distances, and furthermore that the quantum numbers of the exchanged particle are in accord with naive expectations; for the process  $PP \rightarrow PP$  a vector meson is exchanged, whilst for the process  $PV \rightarrow VP$  a pseudoscalar particle is exchanged.<sup>61</sup>

The especially attractive feature of heavy-light systems is that the heavy quarks admit the definition of a relative coordinate, and thereby a local adiabatic potential. Recently, exploratory studies have been made of this potential,<sup>62,63</sup> and evidence for nuclear binding sought, as illustrated in Figure 21. The investigation of this potential is important and more feasible than the measurements of the scattering lengths, because the large scattering lengths for the  $N - N$  system come from a short-range potential. Furthermore, by exploring the potential, we can discover the relative importance of gluon and meson exchange contributions at various distances. Understanding the nature of this potential is also crucial to spectroscopy; are exotic mesons predominantly quark-antiquark-glue hybrid states, or four-quark states?

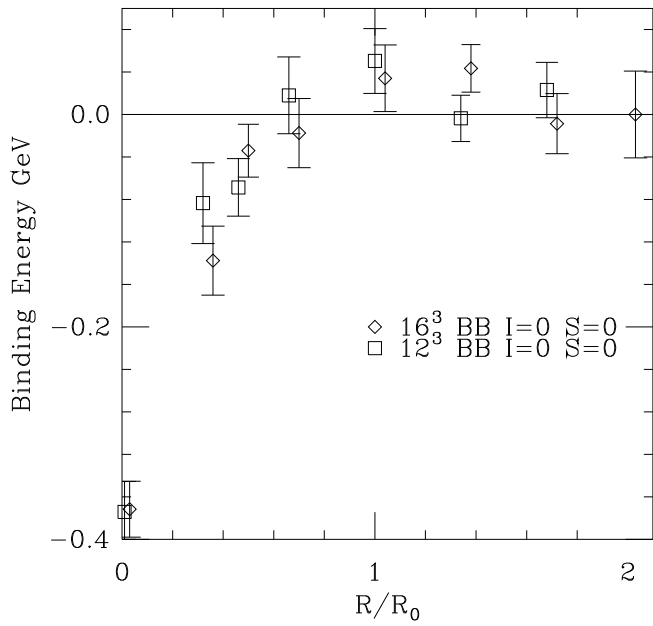


Figure 21: Adiabatic potential between two heavy-light mesons, with the light quarks in an isospin  $I = 0$  and spin  $S = 0$  configuration, from reference<sup>63</sup>. Measurements are obtained in the quenched approximation to QCD, on lattices at  $\beta = 5.7$ . The separations are measured in units of  $R_0 = 0.53$  fm, and the different plotting symbols correspond to different lattice sizes.

## 5 Conclusions

In these lectures I have tried to convey the power of lattice gauge calculations as a means of understanding hadronic physics. There are very many areas that I have not addressed - topology and the role of instantons, finite-temperature and finite-density phase transitions, and, reaching beyond hadronic physics, the calculation of weak-interaction matrix elements and even supersymmetry and gravity. I trust that I have convinced you that lattice gauge theory provides not only an *ab initio* tool for obtaining quantitative results (the spectrum, form factors etc.), but also provides a means of increasing our conceptual understanding of the strong interaction, for example through the study of the nuclear-nuclear force.

## Acknowledgements

I am grateful for helpful discussions with Stefano Capitani, Robert Edwards, Rudolf Fiebig, Nathan Isgur, Xiandong Ji, Frank Lee, and Stephen Wallace. I also thank Jose Goity and staff for their excellent HUGS workshop. This work was supported by DOE contract DE-AC05-84ER40150 under which the Southeastern Universities Research Association (SURA) operates the Thomas Jefferson National Accelerator Facility.

## References

1. K. Wilson, Phys. Rev. **D10** (1974) 2445.
2. S. Duane, A.D. Kennedy, B.J. Pendleton and D. Roweth, Phys. Lett. **B195** (1987) 216.
3. H.B. Nielsen and M. Ninomiya, Nucl. Phys. **B185** (1981) 20; Nucl Phys. **B195** (1982) E541; Nucl Phys. **B193** (1981) 173.
4. P.H. Ginsparg and K.G. Wilson, Phys. Rev. **D25** (1982) 2649.
5. D.B. Kaplan, Phys. Lett. **B288** (1992) 342.
6. Y. Shamir, Nucl. Phys. **B406** (1993) 90.
7. Nucl. Phys. (Proc. Suppl.) **B83** (2000) 224.
8. R. Narayanan and H. Neuberger, Phys. Lett. **B302** (1993) 62; Nucl. Phys. **B412** (1994) 574.
9. R. Narayanan and H. Neuberger, Nucl. Phys. **B443** (1995) 305.
10. R.G. Edwards and U.M. Heller, hep-lat/0005002.
11. K. Symanzik, Nucl. Phys. **B226** (1983) 187; Nucl. Phys. **B226** (1983) 205.
12. B. Sheikholeslami and R. Wohlert, Nucl. Phys. **B259** (1985) 572.
13. G. Heatlie *et al.*, Nucl. Phys. **B352** (1991) 266.

14. C.R. Allton *et al.* (UKQCD Collaboration), Phys. Lett. **B292** (1992) 408.
15. G.P. Lepage and P.B. Mackenzie, Phys. Rev. **D48** (1993) 2250.
16. K. Jansen *et al.*, Phys. Lett. **B372** (1996) 275;
17. M. Lüscher *et al.*, Nucl. Phys. **B478** (1996) 365.
18. M. Lüscher *et al.*, Nucl. Phys. **B491** (1997) 323.
19. R. Sommer, Nucl. Phys. **B411** (1994) 839.
20. H. Wittig (UKQCD Collaboration), Nucl. Phys. (Proc. Suppl.) **42** (1995) 288.
21. C.R. Allton *et al.* (UKQCD Collaboration), Phys. Rev. **D60** (1999) 034507.
22. O. Philipsen and H. Wittig, Phys. Rev. Lett. **81** (1998) 4056.
23. F. Knechtli and R. Wommer (Alpha Collaboration), Phys. Lett. **B440** (1998) 345.
24. P.W. Stephenson, Nucl. Phys. **B550** (1999) 427.
25. P. Pennanen and C. Michael, hep-lat/0001015
26. CP-PACS Collaboration (S. Aoki *et al.*), Phys. Rev. Lett. **84** (2000) 238.
27. UKQCD Collaboration (K.C. Bowler *et al.*), hep-lat/9910022, Phys. Rev. **D** (to appear).
28. S. Sint and P. Weisz, Nucl. Phys. **B502** (1997) 251.
29. R.G. Edwards, U.M. Heller and T.R. Klassen, Phys. Rev. Lett. **80** (1998) 3448.
30. C. Michael, hep-ph/9710249, in Proc. of Advanced Study Institute on Confinement, Duality and Non-Perturbative Aspects of QCD, Cambridge, England, 23rd. June to 4th. July, 1997.
31. C. Morningstar and M. Peardon, Nucl. Phys. (Proc. Suppl.) **42** (1995) 258.
32. C. Morningstar and M. Peardon, Nucl. Phys. (Proc. Suppl.) **53** (1997) 917; Phys. Rev. **D56** (1997) 4043.
33. C. Morningstar and M. Peardon, Phys. Rev. **D60** (1999) 34509
34. E852 Collaboration (D.R. Thompson *et al.*), Phys. Rev. Lett. **79** (1997) 1630; Phys. Rev. Lett. **81** (1998) 5760.
35. G.M. Beliadze *et al.*, Phys. Lett. **B313** (1993) 276; A. Zaitsev, Proc. of HADRON-97, Brookhaven National Laboratory, August 1997.
36. P. Lacock, C. Michael, P. Boyle and P. Rowland (UKQCD Collaboration), Phys. Rev. **D54** (1996)
37. MILC Collaboration (C. Bernard *et al.*), Nucl. Phys. (Proc. Suppl.) **73** (1999) 264.
38. C. Bernard *et al.* Nucl. Phys. (Proc. Suppl.) **53** 228.
39. P. Lacock and K. Schilling (SESAM Collaboration), Nucl. Phys. (Proc.

- Suppl.) **73** (1999) 261.
40. F.X. Lee and D.B. Leinweber, Nucl. Phys. (Proc. Suppl.) **B73** (1999) 258.
  41. H. Hamber and C.M. Wu, Phys. Lett. **B133** (1983) 351; Phys. Lett. **B136** (1984) 255.
  42. S. Sasaki, invited talk at Jefferson Laboratory Workshop on the Physics of Excited Nucleons, Feb. 16-19, 2000, hep-ph/0004252.
  43. Nucl. Phys. (Proc. Suppl.) **73** (1999) 294.
  44. C.V. Christov *et al.*, Prog. Part. Nucl. Phys. **37** (1996) 91.
  45. L. Maiani and M. Testa, Phys. Lett. **B245** (1990) 585.
  46. G. Beccarini *et al.*, Nucl. Phys. **B456** (1995) 271.
  47. M. Göckeler *et al.*, Phys. Rev. **D53** (1996) 2317; Prog. Theor. Phys. Suppl. 122 (1996) 145; Phys. Rev. **D54** (1996) 5705.
  48. H.L. Lai, J. Botts, J. Huston, J.G. Morfin, J.F. Owens, J.W. Qiu, W.K. Tung and H. Weerts, Phys. Rev. **D51** (1995) 4763.
  49. R. Brower *et al.*, Nucl. Phys. (Proc. Suppl.) **53** (1997) 318.
  50. D. Dolgov *et al.*, Nucl. Phys. (Proc. Suppl.) **73** (1999) 300.
  51. M. Göckeler *et al.*, Minireview given at DIS97, Chicago, April 1997, hep-ph/9706502.
  52. S. Capitani *et al.*, Nucl. Phys. (Proc. Suppl.) **79** (1999) 173; Nucl. Phys. **B570** (2000) 393.
  53. M. Lüscher, Commun. Math. Phys. 105 (1986) 153.
  54. M Lüscher, Nucl. Phys. **B354** (1991) 531.
  55. M. Lüscher, Nucl. Phys. **B364** (1991) 237.
  56. M. Göckeler, H.A. Kastrup, J. Westfalen and F. Zimmermann, Nucl. Phys. **B425** (1994) 413.
  57. M. Fukugita, Y. Kuramashi, M. Okawa, H. Mino and A. Ukawa, Phys. Rev. **D52** (1995) 3003.
  58. S. Aoki *et al.* (JLQCD Collaboration), Nucl. Phys. (Proc. Suppl.) **B83** (2000) 241. hep-lat/9911025, to appear in the Proceedings of Lattice 99, Pisa, Italy.
  59. H.R. Fiebig, H. Markum, K. Rabitsch, and A. Mihály, Few Body Systems (Suppl.) 10 (1999) 467.
  60. D.G. Richards, Nucl. Phys. (Proc. Suppl.) **B9** (1989) 181.
  61. D.G. Richards, D.K. Sinclair, and D. Sivers, Phys. Rev. **D42** (1990) 3191.
  62. A. Mihály, H.R. Fiebig, H. Markum and K. Rabitsch, Phys. Rev. **D55** (1997) 3077.
  63. C. Michael, and P. Pennanen (UKQCD Collaboration), Phys. Rev. **D60** (1999) 054012.